Microscopic modelling of reverse biased Schottky diodes: influence of non-equilibrium transport phenomena

2007 Semicond. Sci. Technol. 22 1003

(http://iopscience.iop.org/0268-1242/22/9/005)

Semicond. Sci. Technol. **22** (2007) 1003–1009 doi:10.1088/0268-1242/22/9/005

Microscopic modelling of reverse biased Schottky diodes: influence of non-equilibrium transport phenomena

Elena Pascual, Raúl Rengel and María J Martín

Departamento de Física Aplicada, Universidad de Salamanca, 37008 Salamanca, Spain

E-mail: elenapc@usal.es

Received 18 May 2007, in final form 18 June 2007
Published 6 August 2007
Online at stacks.iop.org/SST/22/1003

Abstract
A Monte Carlo investigation of charge transport—including quantum tunnelling effects—across Schottky barriers (both n-type and p-type) in the reverse bias regime is presented. The effect of the variation of different quantities (such as the barrier height or the temperature) over the current density is discussed and extensively analysed. A thorough study of different internal magnitudes such as carrier density, electric field, etc. together with velocity distribution functions and the density of scattering mechanisms has been carried out. In this way, a detailed description of microscopic charge transport in the depletion region associated with the Schottky contact is attained. Results evidence important quasi-ballistic characteristics in the region closer to the contact, thus becoming an important issue to be tackled in the modelling of Schottky-based devices with reverse biased junctions.

1. Introduction

Nowadays we are in an extremely interesting moment in the development of the microelectronics industry. The evolution of the scaling of silicon MOSFET devices (which account for the largest share in the integrated circuits market) faces great challenges when reaching extremely reduced dimensions, in the nano-metric scale. In particular, the predictions of the semiconductor industry based on the International Technology Roadmap for Semiconductors [1] point out that we are going into the age of the device scaling limited by the properties of their constituent materials.

In order to settle the problems associated with the downscaling of conventional MOSFETs, different alternatives are proposed, such as hetero-junction transistors (especially those of silicon–germanium alloy) [2], the silicon-on-insulator technology (SOI) [3], strained silicon MOSFETs [4, 5], double-gate MOSFETs [6], or the so-called Schottky barrier MOSFET (SB-MOSFET) [7, 8], where the doped source and drain junctions are replaced by Schottky contacts. Recently, the interest in these SB-MOSFETs has remarkably increased due to their particular properties. For example, the use of metallic S/D allows providing a significantly lower access resistance together with extremely abrupt interfaces at those contacts, thus allowing an improved scalability and reduced short channel effect [8]. Moreover, the poor minority-carrier injection from the source practically eliminates the parasitic bipolar action [9], which is of particular relevance for ultra-scaled devices. Since no high temperature spike or flash anneals are required to activate S/D dopants, a lower thermal budget is necessary, which is desirable for the integration with other solutions such as strained Si or SiGe channels [10]. In general, the fabrication process is fully CMOS compatible [8]. The basic principle of operation of SB-MOSFETs is the following: in the on-state (which is controlled by the gate contact) tunnelling dominates and together with field emission is responsible for the injection of carriers into the channel. The off-state is completely guaranteed by the built-in Schottky barrier at the source contact, so a proper operation is achieved [11]. In the SB-MOSFET the source contact (which controls the injection of carriers into the channel) is under the reverse bias condition for accumulation mode devices [11], and in inversion mode transistors the junction leakage current across the reverse biased drain Schottky contact may also play an important role [8].

To achieve an exhaustive comprehension of the physics of transport in such devices, it is first essential to perform an in-depth study of Schottky barriers, with particular attention to the reverse bias regime. To this end, advanced modelling tools

such as the Monte Carlo method applied to the simulation of electronic devices becomes [12] of great interest, since it reproduces the microscopic nature of electronic charge transport. This is of particular importance since, as will be discussed afterwards, the depletion region that appears adjacent to the Schottky contact when a reverse bias is applied shows strongly non-equilibrium features that may affect the electronic transport inside the device. Consequently these effects must be adequately modelled, bearing in mind that in SB-MOSFETs such phenomena will come together with ballistic effects inherent to the short dimensions of the device channel [13]. The Monte Carlo method is the ideal tool to carry out this study, since it incorporates in a natural way these kinds of effects and may provide valuable information about transport processes through the study of internal quantities such as concentration, energy, electric field profiles, average velocity distribution functions, etc. Moreover, a careful consideration of the charge injection and absorption must be carried out, considering not only thermionic effects but also quantum tunnelling effects [14]. The temperature and the barrier height are parameters that may strongly affect the injection and absorption through the Schottky contact, so their importance must also be analysed.

In this work, we present a Monte Carlo simulation of Schottky barrier diodes (both n-type and p-type) under the reverse biased regime. Previous works have dealt with the modelling of Schottky barrier silicon diodes using Monte Carlo simulators: the analysis of the diode under forward bias conditions is developed in [15]; the focus of electron velocity dispersion in the channel of devices under reverse bias is given in [16] and a study of the reverse current–voltage characteristics is performed in [17]; however, to the authors' knowledge an in-depth microscopic study of the influence on the electronic transport of the non-equilibrium depletion region under reverse bias conditions has not been previously addressed by using this simulation technique. The paper is organized as follows. In section 2 we present the main details about the structures under study and our Monte Carlo simulator, presenting also the injection/absorption model implemented to treat quantum tunnelling effects. Next, in section 3 we report not only the comparison between the simulation results and the experimental data but also a complete analysis of the influence of the barrier height in section 3.1, and of the temperature in section 3.2; moreover, a study of the internal magnitudes (including average velocity, energies, electric fields, scattering mechanisms and velocity distribution functions) is also reported in section 3.3 in order to examine the features of transport inside the device. Finally, in section 4 the main conclusions are presented.

2. Simulated devices and Monte Carlo procedure

The simulated structure corresponding to the experimental Schottky barriers under test is shown in figure 1. Both n^+-n-silicide and p^+-p-silicide structures have been taken into account. An ohmic contact [18] is placed at the left end of the structure, while the Schottky contact is at the right; as specified in table 1, several barrier heights and doping profiles for electrons and holes have been modelled, corresponding to different metallic silicide compounds, such as $ZrSi_2$, RhSi and PtSi [19], for which experimental measurements were available at several different temperatures. The barrier height is defined [14], in the case of electrons, as the difference between the metal work function and the electron affinity of the semiconductor:

$$q\Phi_{\mathrm{Bn}} = q(\Phi_M - \chi) \tag{1}$$

where Φ_M is the metal work function and χ is the electron affinity of the semiconductor. In the case of the barrier to holes $q\Phi_{\mathrm{Bp}}$ the semiconductor gap E_g must also be considered:

$$q\Phi_{\mathrm{Bp}} = E_g - q(\Phi_M - \chi). \tag{2}$$

The numerical simulations have been carried out by means of a Monte Carlo device simulator, one dimensional in the real space and three dimensional in the momentum space. Our Si band model includes non-parabolic X and L valleys of the conduction band, and two non-parabolic bands (heavy and light) of the valence band; more details can be found in [20, 21]. The study is carried out in the [1 0 0] crystallographic direction. The scattering mechanisms considered in the simulation are the following: optical phonons, acoustic phonons and impurity scattering mechanisms. The time step considered to self-consistently solve the Poisson equation is 1 fs; hence, the total simulation time varies from 1.5 to 3 ns depending on the bias point and the barrier height. The cells in which the simulated structure is divided are 10 nm long; a refined mesh near the Schottky contact is considered to study in depth the features of transport in that region. Due to the relatively high barriers studied (see table 1), the current density involved in transport in the reverse regime of operation is expected to be very small. As a consequence, to maintain the adequate statistical resolution in the depletion region adjacent to the Schottky contact, the statistical enhancement technique based on an expansion/compression algorithm has been considered [15]. By using this methodology, we can achieve an approximately constant number of 100 particles per each cell of the simulated Monte Carlo structure.

To properly consider current transport phenomena through the Schottky barrier, specific features for

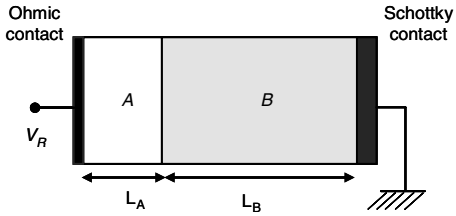

Figure 1. Scheme of the simulated structures for the Schottky diodes under study. The characteristics of the regions A and B are reflected in table 1.

Table 1. Characteristics of the different simulated structures (silicide type, doping, dimensions and Schottky barrier heights).

Structure	A Doping (cm^{-3})	L_A (μm)	B Doping (cm^{-3})	L_B (μm)	Barrier height (eV)
Si-n/$ZrSi_2$	10^{17}	0.2	3.5×10^{15}	0.8	0.55
Si-n/RhSi	10^{17}	0.2	3.5×10^{15}	0.8	0.78
Si-n/PtSi	10^{17}	0.2	3.2×10^{15}	0.8	0.87
Si-p/RhSi	10^{17}	0.2	9.0×10^{17}	0.8	0.33

implementing tunnelling and thermionic processes (both injection, from silicide to semiconductor, and absorption, from semiconductor to silicide) have been included in our Monte Carlo simulator. These four different contributions to the total current crossing the Schottky barrier have been directly evaluated by counting all the injected or absorbed particles involved in the simulation of the Schottky interface, and not by analytical or numerical calculations. Injection and absorption are treated in different ways. Considering injection from the silicide to the semiconductor, we perform a discretization of the incident energies, distinguishing two ranges: thermionic energies (relative to those particles with incident energy higher than the barrier height) and tunnelling energies (with values lower than the barrier height). From the theoretical expression of the current injected from metal to semiconductor [17, 22], the number of particles to be injected at each time step Δt can be obtained as follows:

$$N_{\text{inj}} = \frac{A^* T \Delta t}{K_B} \sum_{i=1}^{n_{\text{eng}}} \frac{T_{ms}(E_i) f_m(E_i)[1 - f_s(E_i)]\Delta E_i}{PW_j} = \sum_{i=1}^{n_{\text{eng}}} \frac{Q_i}{PW_j} \tag{3}$$

where f_m and f_s are the Fermi–Dirac distribution functions in the silicide and in the semiconductor, A^* is the Richardson's constant, T is the temperature and K_B is the Boltzmann constant. n_{eng} is the total number of incident energy regions considered in the discretization, E_i is the value of the incident energy inside the metallic silicide and PW_j is the equivalent particle weight (this is, the number of real carriers that each simulated particle represents, which depends on the cell j to be injected according to the expansion/compression algorithm). Q_i is the charge injected at each energy region. T_{ms} corresponds to the transmission coefficient from the silicide to the semiconductor.

In order to evaluate T_{ms}, the WKB approximation [23] has been considered. It has been recently shown that the WKB approach can correctly predict (as compared to other more elaborated but CPU consuming methods such as the Airy transfer matrix [24]) the total current through the Schottky barrier by means of an adequate consideration of the model parameters (for instance, the Richardson constant) [25]. The WKB transmission probability depends not only on the incident energy but also on the potential band profile which in our case is self-consistently provided by the Monte Carlo simulation. It must also be remarked that the potential profile is modified by the image charge effect, slightly reducing the effective barrier height at the region near the contact, according to the following expression [26]:

$$\Delta\Phi = \sqrt{\frac{q\xi}{4\pi\varepsilon_s}} \tag{4}$$

where q is the magnitude of the electronic charge, ε_s is the permittivity of the semiconductor material and ξ is the electric field. Once all these quantities are determined (potential profile, transmission coefficient and the number of particles to be injected) the injection itself must be carried out in the Monte Carlo simulation. The injected energy region for each individual particle is properly chosen according to the distribution of the injected charge by using a random number r (with probability uniformly distributed between 0 and 1):

$$\sum_{k=1}^{i} \frac{Q_k}{PW_j} < r\ N_{\text{inj}} < \sum_{k=1}^{i+1} \frac{Q_k}{PW_j}. \tag{5}$$

The thermionic particles injected are placed in the nearest cell to the Schottky contact with the following value of the wave vector perpendicular to the contact surface:

$$k_x = \sqrt{\frac{2m_x^*}{\hbar}\left(\frac{1}{2}K_B T + E_i - q\Phi_B\right)} \tag{6}$$

where m_x^* is the effective mass of the corresponding injection valley along the longitudinal axis and $q\Phi_B$ is the effective barrier height. k_y and k_z (components parallel to the contact) account for the remaining thermal energy in the other two directions. Those particles injected by the tunnelling effect are placed inside the device at the turning point determined by their incident energy, with an initial value of k_x equal to zero [27] while the corresponding values of k_y and k_z are assigned in an analogous way to the thermionic case.

A different procedure is followed to treat the absorption processes [16]. Particles reaching the Schottky contact with enough energy to surmount the barrier are thermionically absorbed, leaving the simulated structure. The transmission coefficient from the semiconductor to the metallic silicide (T_{sm}, calculated in an analogous way than T_{ms}) is needed to evaluate if a particle is absorbed or not by the tunnelling effect. The particles prone to be absorbed by this effect are those reaching a turning point at which the component of the wave vector parallel to the tunnelling path equals zero. A rejection technique is used to determine if the particle is absorbed or not: if a random number (with probability uniformly distributed between 0 and 1) is lower than T_{ms}, then the particle is absorbed; otherwise it will be reflected.

In order to calibrate the injection/absorption model, several simulations were carried out under equilibrium conditions, for which injection and absorption processes must compensate in order to provide the total zero current. In accordance with the results shown in [25], the Richardson constant was considered as the fitting parameter in the WKB model, thus finding a value equal to 200 A cm^{-2} K^{-2} for n-type diodes and 60 A cm^{-2} K^{-2} for p-type ones, which was kept constant for all the simulations and for all temperature conditions.

3. Results and discussion

3.1. Barrier height dependence

In figure 2 we show the experimental current density–reverse voltage (J–V_R) characteristics [19] together with the Monte Carlo results for three different barrier heights at 300 K; as shown in the graph, an excellent agreement is obtained between both sets of data. As the barrier increases, the total current density gets significantly reduced, as expected by the exponential dependence of the total current on the barrier height described by the classical thermionic emission–diffusion (TED) theory [28].

To properly ponder the influence of the barrier height on the injected current, we show in figure 3(*a*) the percentage of

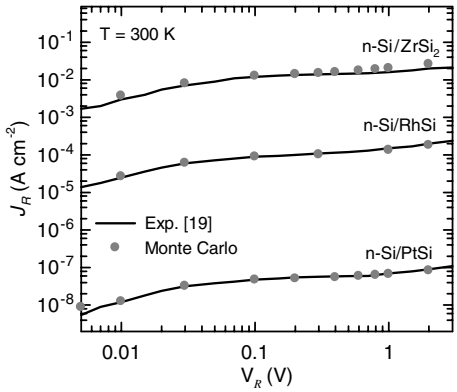

Figure 2. Reverse J–V_R characteristics at 300 K for three different barrier heights corresponding to n-Si/$ZrSi_2$, n-Si/RhSi and n-Si/PtSi. Lines correspond to experimental data and symbols to the Monte Carlo results.

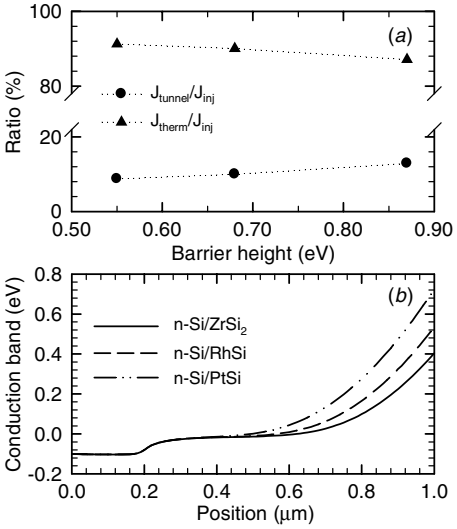

Figure 3. Percentage of tunnelling and thermionic injected currents (*a*) and conduction band profiles for the n-type contacts at 300 K and $V_R = 0.1$ V (*b*).

thermionic and tunnelling components over the total injected current for $V_R = 0.1$ V. As can be seen, the thermionic current accounts for most of the total injected current; however, its relative importance gets reduced when the barrier height increases, while the contribution of the tunnelling current to the total injected current augments. For a better understanding of this behaviour, we present in figures 4(*a*) and (*b*) the transmission coefficient T_{ms} and the injected charge profile for the three barrier height values considered. According to the WKB approximation, the transmission coefficient equals 1 for energies higher than $q\Phi_B$, bearing in mind that the effective barrier height is slightly reduced due to the image charge effect. In this energy range, an exponential behaviour of the injected charge is observed (figure 4(*b*)), following the tail of the Fermi–Dirac distribution function for electrons inside the silicide. In the case of tunnelling energies (those lower than $q\Phi_B$) a sharp drop of the transmission coefficient is observed, that yields, together with the metallic silicide occupancy function, the tunnelling injected charge profile shown in figure 4(*b*). The greater number of particles injected

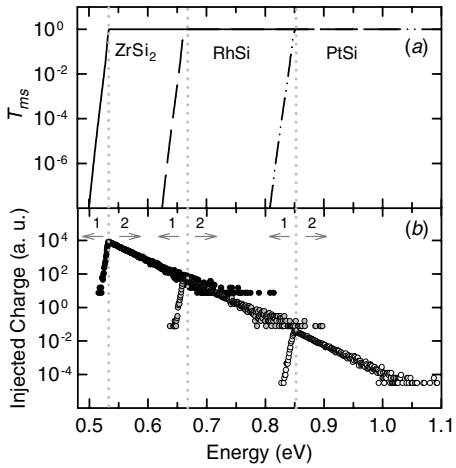

Figure 4. Transmission coefficient (*a*) and injected charge profile (*b*) provided by the Monte Carlo simulation as a function of the incident energy for the n-type contacts at 0.1 V and 300 K. '1' indicates the tunnelling energies and '2' the thermionic ones.

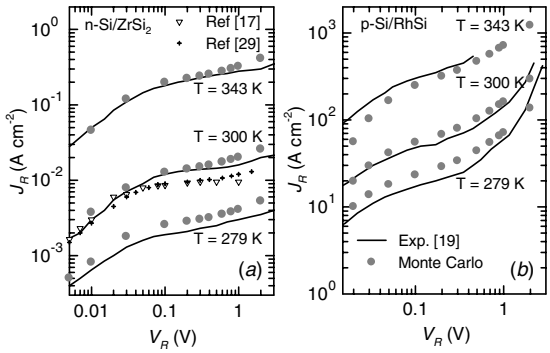

Figure 5. J–V_R characteristic of the n-Si/$ZrSi_2$ diode (*a*) and the p-Si/RhSi device (*b*) both for 279, 300 and 343 K. The results of [17] and [29] for the n-Si/$ZrSi_2$ diode at 300 K are shown for comparison.

by tunnelling effect correspond to injection energies at the vicinity of the barrier height value, which is due to a narrower tunnelling path in this case determined by the conduction band profile (figure 3(*b*)). When the barrier height gets augmented, the injected charge drastically lowers since the energies needed to inject particles are logically higher and therefore correspond to energetic states inside the silicide less occupied. The higher $q\Phi_B$ also affects the barrier profile as can be observed in figure 3(*b*), the tunnelling processes being favoured in comparison to the thermionic ones since the barrier gets thinner, thus reducing the tunnelling path. Anyway, for the highest barrier the thermionic injected charge is still much more important than the charge injected by quantum tunnelling, as expected by the low doping of the semiconductor [14]. If a higher doping is considered in the semiconductor, tunnelling components shall be considerably augmented due to a thinner Schottky barrier achieved in that case.

3.2. Influence of the temperature

The influence of the temperature on the reverse current is evidenced in figure 5, which shows the J–V_R characteristics corresponding to both n-type and p-type diodes at 279, 300 and

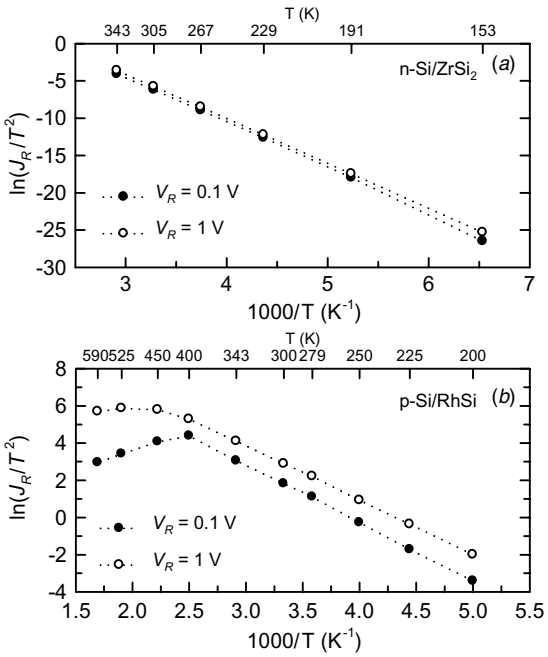

Figure 6. Monte Carlo results for the Arrhenius plot of the structures under study: n-Si/$ZrSi_2$ (*a*) and p-Si/RhSi (*b*) contacts at two different applied voltages, 0.1 and 1 V.

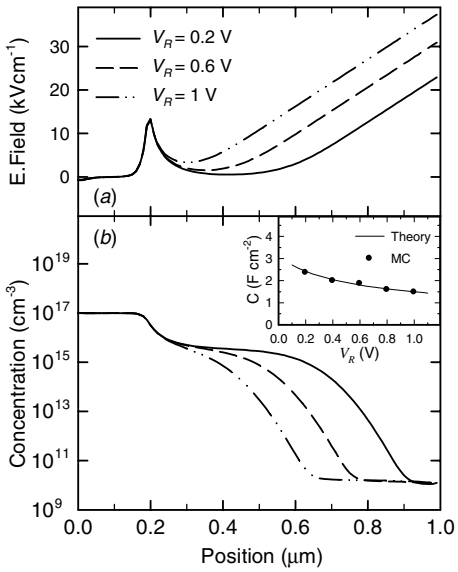

Figure 7. Electric field (*a*) and carrier concentration profiles (*b*) for the n-Si/$ZrSi_2$ diode under several reverse voltages (0.2, 0.7 and 1 V) at 300 K. Inset of figure 7(*b*) shows the device capacitance as a function of the reverse applied voltage, including the Monte Carlo data (symbols) and the theoretical result for a metal-to-semiconductor junction [14] (solid line).

343 K. Figure 5(*a*) corresponds to the simulations of a barrier to electrons (n-Si/$ZrSi_2$ contact) and figure 5(*b*) to those of a barrier to holes (p-Si/RhSi contact), showing both of them a remarkable agreement between the experimental data and the Monte Carlo results. In order to allow the comparison with previous works, the Monte Carlo results of [17] and the numerical ones of [29] have also been added. As can be observed the reverse current initially increases with V_R; this is due to the progressive loss of importance of the absorption current components, so for reverse voltages upper than 0.1 V, carrier injection is dominant, with a growing weight of the tunnelling component under high reverse applied voltages [30], which is more remarkable in the case of the p-type diode (with a higher doping in the semiconductor).

Once that the experimental J–V_R curves have been properly reproduced, it is interesting to evaluate the current temperature dependence by means of the Arrhenius plot, which is a very commonly used method to experimentally determine the value of the barrier height [11]. The Arrhenius plots for two different reverse applied voltages (0.1 and 1.0 V) in the case of n-Si/$ZrSi_2$ and p-Si/RhSi contacts are shown in figure 6.

In figure 6(*a*), we show the Monte Carlo results for the n-type diode; in this case (for a relatively high barrier and reverse applied voltages lower than 1 V) the reverse current follows a Schottky law [14] in the whole temperature range. As can be observed, there are not many differences between the current values for the two reverse bias voltages shown, which belong to a bias region where thermionic injection is dominant, being so the total current almost constant (see figure 5(*a*)). However, in the case of the p-type structure (figure 6(*b*)) important differences are found. In this case, two temperature regions can be clearly distinguished. The first one corresponds to temperatures lower than 400 K for $V_R =$ 0.1 V and 450 K for $V_R = 1.0$ V, for which an exponential decay as a function of T^{-1} is observed. In the second region (for temperatures higher than those previously mentioned) the Schottky law is not obeyed and a decrease of current is obtained as the temperature is raised, thus appearing a maximum in the Arrhenius plot. This behaviour is due to the increase of the silicon resistance and a decrease of the Schottky barrier resistance as the temperature is augmented [11]. In this case, there is a noticeable difference between the current values corresponding to the two curves shown, which is due to the fact that tunnelling injection has a higher relevance than in the previous case, thus achieving the rise of the total current for low reverse voltages applied as reflected in figure 5(*b*).

3.3. Non-equilibrium transport

Let us now examine in detail the features of transport at the proximity of the Schottky contacts by means of the analysis of different quantities provided by our Monte Carlo simulator. Figure 7 shows the electron concentration and the electric field profiles for several values of V_R in the case of the n-Si/$ZrSi_2$ contact at 300 K. As V_R is raised, nearby the contact a positive and increasing electric field appears opposing to the movement of electrons towards the Schottky interface (figure 7(*a*)). The concentration profile (figure 7(*b*)) shows the existence of a depletion region, which gets wider with the applied reverse bias due to the large electric field which pushes the electrons away from the Schottky contact. The variation of the total charge inside the device with the applied voltage is evidenced through the study of the capacitance, which is shown in the inset of figure 7(*b*). This capacitance has been found to be inversely proportional to the space-charge width, which is in good agreement with the theory for metal-semiconductor junctions [14]. Therefore, it can be concluded that the charge

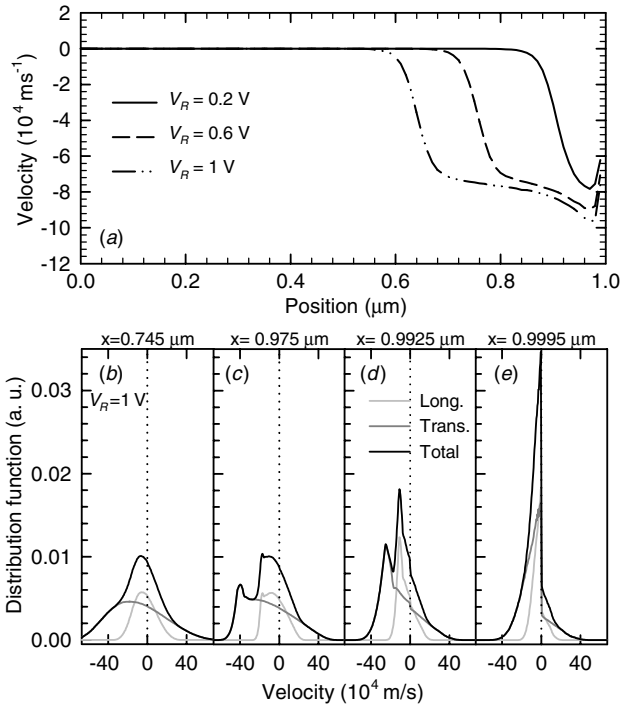

Figure 8. Velocity profile (*a*) of the n-Si/$ZrSi_2$ diode under the same simulation conditions as in figure 7. Distribution function of the velocity of carriers at several locations indicated on the graph for $V_R = 1$ V (*b*), (*c*), (*d*), (*e*).

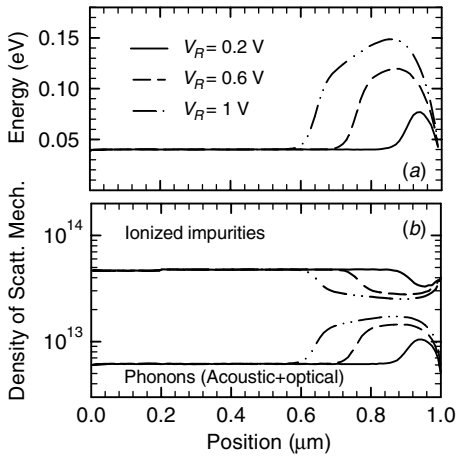

Figure 9. Energy profile (*a*) and density of scattering mechanisms with impurities, acoustic phonons and optical phonons (*b*) for the n-Si/$ZrSi_2$ diode under the same bias and temperature conditions as in figure 7.

injected by the Schottky contact does not significantly affect the electrostatics inside the device. We have also studied the profiles of these magnitudes for the simulated p-type structure (not shown in the figures), obtaining an analogous behaviour but with a narrower depletion region as a consequence of the higher doping of the semiconductor. From now on, we shall focus on the analysis of charge transport in the n-type structures under consideration, for which a wider and significant non-equilibrium space-charge region is presented.

Figure 8(*a*) shows the average velocity profile for several reverse applied voltages. At the depletion region (which is highly resistive), carriers injected from the silicide to the semiconductor are rapidly accelerated due to the previously shown large electric field and acquire elevated velocity values until a maximum is reached; note that the average velocity is negative since electrons are being drifted from right to left in the simulated structure. Carriers finally leave this depletion region (which extends several hundreds of nm) and reach a quasi-equilibrium situation. To examine in depth the behaviour of the injected electrons, from the data recorded for the ensemble of simulated particles we have also calculated the velocity distribution function at several locations inside the semiconductor. In figures 8(*b*)–(*e*) we show the results for V_R equal to 1.0 V; the injection processes are dominant for this reverse voltage value, thus yielding a distribution function at the location closer to the contact which is approximately a negative hemi-Maxwellian (figure 8(*e*), the origin for the *x*-axis is taken at the ohmic contact). At this point, the specific features of the conduction band must be taken into account, because depending on the valley in which the carriers are injected their effective mass will be substantially different and so the action of the electric field. Electrons in longitudinal X valleys of the conduction band present an elevated effective mass (0.91 m_0) and consequently acquire less velocity; in contrast, carriers in the 'light' transversal valleys (mass equal to 0.19 m_0) get higher velocities. This translates into the appearance of two peaks in the velocity distribution function as the carriers move away from the Schottky contact towards the left (figure 8(*d*)). Each of these peaks is associated with electrons inside longitudinal valleys (the maximum at lower velocities) and in the transversal ones (maximum at higher velocities). The velocity values corresponding to these peaks are quite close to the ones expected in a purely ballistic regime of transport. For instance, 25 nm away from the contact surface (figure 8(*c*)), the 'longitudinal' peak takes place at 1.7×10^5 m s^{-1} and the 'transversal' peak is located at 4×10^5 m s^{-1}. In a completely ballistic picture [31] carriers in the longitudinal valleys should have reached a velocity equal to 1.95×10^5 m s^{-1} and electrons in the transversal valleys a velocity equal to 4.4×10^5 m s^{-1}, which indicates that only a very few scattering mechanisms have occurred. Therefore we can assert that in the space-charge region, up to some tens of nm close to the Schottky contact, the transport of injected carriers from the silicide to the semiconductor presents strongly quasi-ballistic features. Going far away from the contact, the velocity peaks tend to smooth and finally, the distribution function approaches a full Maxwellian (figure 8(*b*)).

In order to explain this, we have also examined the energy profile and the density of scattering mechanisms as a function of the position, shown in figure 9. As the carriers are injected into the semiconductor, energies well over the thermal one are reached (figure 9(*a*)), in correspondence with the aforementioned increase of the average velocity. When carriers leave behind the space-charge region, their average energy drops to reach the thermal value. The electron energy is interrelated to the scattering probability, the density profile of which is shown in figure 9(*b*). The scattering density corresponding to ionized impurities is higher than that of acoustic and optical phonons along the entire device; however, the anisotropic nature of this kind of scattering means that,

individually speaking, its effect is of less importance than the effect of the isotropic phonon scattering. When the electrons enter into the device, the initial rise of energy at the depletion region induces an important increase of isotropic scattering mechanisms with phonons. Such scattering with phonons tends to perform a significant relaxation action over the momentum and the energy. In contrast, the average velocity and energy are increased by the electric field. Both effects compete with each other, but finally the influence of phonon scattering tends to impose few hundreds of nm away from the interface (where in addition the electric field is smaller) thus achieving the quasi-equilibrium situation, which takes place further away from the Schottky contact as V_R is higher. The relaxation action of phonons over the electron momentum also explains the smoothing of the velocity distribution function as electrons get away from the Schottky interface. Moreover, the existence of these scattering mechanisms yields the turning back of some carriers, which produces the positive tail of the distribution function near the contact (figure 8(*e*)).

The rise of phonon scattering in the space-charge region produces also an increase of the occupancy of the longitudinal X valley, which has been checked to reach a maximum value equal to 37% of the total occupancy. The thermalization of carriers is also reflected in the valley occupancies once the depletion region has been exceeded; in the quasi-equilibrium region inside the semiconductor, valleys finally become equally populated.

4. Conclusions

A Monte Carlo investigation of transport through Schottky barriers in n-type and p-type contacts has been presented. An injection/absorption algorithm based on the WKB approach has been developed and incorporated into a 1D Monte Carlo simulator in order to properly reproduce the physics of transport inside the device under reverse bias conditions. The simulated J–V_R characteristics show an excellent agreement with the experimental measurements. The study of the influence of the barrier height has evidenced the decrease of the injected charge with higher values of $q\Phi_B$ because of the higher energies necessary to perform the injection; moreover, it has been observed that the contribution of tunnelling to the total injection slightly increases in the case of higher barriers. The temperature effect over the charge transport has been analysed by means of the Arrhenius plot. While for relatively high barriers (as in the case of the simulated n-type structures) the J/T^2 ratio shows an exponential dependence on T^{-1} in the whole temperature range, for the investigated p-type diode (with low barrier height) it has been shown that the Schottky law is not obeyed at high temperatures. Carrier density profiles, energy and velocity dependences and electric fields have been extensively discussed, together with the analysis of the velocity distribution function for a reverse applied voltage and the scattering density profile. Results have evidenced the strong quasi-ballistic nature of charge transport at the vicinity of the Schottky contact, a very important fact to consider in the analysis of the behaviour of SB-MOSFETs with gate lengths of few tens of nm.

Acknowledgment

This work was supported by research project METAMOS (IST-016677) financed by the European Commission.

References

[1] The International Technology Roadmap for Semiconductors 2005 San Jose, CA, http://public.itrs.net
[2] Lee M L and Fitzgerald E A 2003 *IEDM '03 Technical Digest. 18.1.1*
[3] Shahidi G G 2002 *IBM J. Res. Dev.* **46** 121
[4] Aubry-Fortuna V *et al* 2006 *Semicond. Sci. Technol.* **21** 422
[5] Fossum J G and Zhang W M 2003 *IEEE Trans. Electron Devices* **50** 4
[6] Bufler F M *et al* 2004 *Semicond. Sci. Technol.* **19** S122
[7] Connelly D, Faulkner C and Grupp D E 2003 *IEEE Trans. Electron Devices* **50** 1340
[8] Larson J M and Snyder J P 2007 *IEEE Trans. Electron Devices* **53** 1048
[9] Sugino M, Akers L A and Rebeschini M E 1982 *IEDM Tech. Dig.* p 462
[10] Ikeda K *et al* 2002 *IEEE Electron Device Lett.* **23** 670
[11] Dubois E and Larrieu G 2004 *J. Appl. Phys.* **97** 729
[12] Jacoboni C and Lugli P 1989 *The Monte Carlo Method for Semiconductor Device Simulation* (Viena: McGraw-Hill)
[13] Ahn C and Shin M 2007 *IEEE Trans. Nanotechnol.* **5** 278
[14] Sze S M 1981 *Physics of Semiconductor Devices* 2nd edn (New York: Wiley)
[15] Martín M J, González T, Pardo D and Velázquez J E 1997 *Semicond. Sci. Technol.* **11** 380
[16] Matsuzawa K, Uchida K and Nishiyama A 2000 *IEICE Trans. Electron.* **E83-C** 1212
[17] Sun L, Liu X Y, Liu M, Du G and Han R 2003 *Semicond. Sci. Technol.* **18** 576
[18] González T and Pardo D 1997 *Solid-State Electron.* **39** 555
[19] Andrews J M and Lepselter M P 1970 *Solid State Electron.* **13** 1011
[20] Martín M J, Velázquez J E and Pardo D 1997 *J. Appl. Phys.* **79** 7975
[21] Martín M J, Pérez S, Pardo D and González T 2001 *J. Appl. Phys.* **90** 1582
[22] Huang C K, Zhang W E and Yang C H 1998 *IEEE Trans. Electron Devices* **45** 842
[23] Bransden B H and Joachain C J 1987 *Introduction to Quantum Mechanics* (New York: Longman Scientific & Technical)
[24] Lui W W and Fukuma M 1987 *J. Appl. Phys.* **50** 1555
[25] Rengel R, Pascual E and Martín M J 2007 *IEEE Electron Dev. Lett.* **28** 171
[26] Neamen D A 1992 *Semiconductor Physics and Devices* (Boston: Irwin)
[27] Shen M, Saiking S and Cheng M-C 2004 *J. Appl. Phys.* **97** 4319
[28] Crowell C R and Sze S M 1977 *Solid-State Electron.* **9** 1035
[29] Matsuzawa K, Uchida K and Nishiyama A 2000 *IEEE Trans. Electron Devices* **47** 103
[30] Pascual E, Rengel R and Martín M J 2007 Monte Carlo analysis of tunneling and thermionic transport in a reverse biased Schottky diode *7th Spanish Conference on Electronic Devices (Madrid)*
[31] Ashcroft N W and Mermin N D 1977 *Solid State Physics* (Philadelphia: Saunders College)